174 **MAXIMIZING THE BENEFITS OF ADAPTIVE SCANNING FOR WEATHER RADARS: THE DEVELOPMENT OF AN ADAPTIVE WEATHER SENSING FRAMEWORK TO INVESTIGATE THE EFFECTIVENESS OF TASK-SPECIFIC UPDATE TIME ASSIGNMENTS**

Tian-You Yu[1,2,3]*, **Sebastian Torres**[1,2,4,5], **Ricardo Reinoso-Rondinel**[1,2] **and Damian Vigouroux**[1]
[1] School of Electrical and Computer Engineering, University of Oklahoma, Norman, OK
[2] Atmospheric Radar Research Center, University of Oklahoma, Norman, OK
[3] School of Meteorology, University of Oklahoma, Norman, OK
[4] Cooperative Institute for Mesoscale Meteorological Studies, University of Oklahoma, Norman, OK.
[5] National Severe Storms Laboratory, NOAA, Norman, OK

1. Introduction

The WSR-88D surveils the atmosphere by mechanically rotating a reflector antenna 360° in azimuth at a pre-defined number of elevation angles. These conventional sensing patterns are known as volume coverage patterns (VCP) (Crum and Alberty 1993), which takes 4–5 min. for storms. However, update times of 4–5 min may not be sufficient to detect and monitor fast-evolving weather phenomena. One plausible solution is adaptive weather sensing. In this work, two radar functions of storm tracking and surveillance are considered. The goal of adaptive weather sensing is to revisit different storms with different and fast update times, while the quality of the data as for conventional sensing is maintained. The beam agility offered by the phased array radar (PAR) is well-suited for performing such focused observations.

A framework for adaptive weather sensing is proposed to execute tasks of tracking storm cells and weather surveillance. In order to schedule multiple tasks that are competing for radar resources, a time balance (TB) scheduling algorithm is proposed by Reinoso-Rondinel et al. (2010). In addition, two quality measures are introduced to evaluate the performance of adaptive weather sensing. In this work, reflectivity fields observed by operational WSR-88D radars were used to simulate high-temporal-resolution PAR observations in order to demonstrate the feasibility of the proposed framework. With these simulations, we can demonstrate that a multifunction PAR can adaptively scan a number of regions of interest (storm cells) with task-specific update times. This can be accomplished with no degradation in data quality and higher-temporal resolution compared to conventional radar, while surveillance is maintained to ensure the tracking of developed storms and the detection of new formations. However, the performance of adaptive weather sensing depends on the requested update time for each task. Optimal update times were estimated by solving a constrained optimization problem. The performance of adaptive weather sensing using optimal update times is compared to that from a simple and intuitive rule of uniform update

*Corresponding Author: T.-Y. Yu (tyu@ou.edu), School of Electrical and Computer Engineering, University of Oklahoma, 110 W. Boyd, DEH 433, Norman, OK 73019, USA

times for all the tasks.

2. Framework for adaptive weather sensing

The framework is designed to be a close-loop modular system, which obtains information about the environment perceived by the radar and dynamically adjusts its operation accordingly. The proposed framework is shown in Figure 1, which consists of four main processes: (1) storm cell identification, (2) storm-cell tracking, (3) task configuration, and (4) scheduler. Simply speaking, the process of storm identification uses reflectivity data from the surveillance task, detects storm cells, and estimates their location and extent (beam coverage) using imaging processing. The storm-cell tracking process confirms the newly identified storm cells, associates the storm cells in time, and predicts the beam coverage for future tracking executions. The task configuration calculates the time needed to execute each task, regulates the requested update times for each task, and determines the sensing mode. In other words, the PAR will perform the conventional volume coverage pattern if no gain from adaptive sensing is anticipated. The process of scheduling the requested tasks is done by the scheduler. In this work, the TB scheduler was used to arrange these competing tasks to achieve the requested occupancy of each task (Reinoso-Rondinel et al. 2010). At this point, the information of where and when to steer the beam has been determined.

The block depicted with dotted lines is called the radar operation and consists of the PAR, the display of surveillance, the display of storm tracking, and the user inputs indicated by the cyan, green, red, and yellow blocks respectively. The PAR executes the tasks of surveillance and storm tracking by steering the radar beam to specific locations in the specified order after receiving a sequence of scan commands from the scheduler. A single stationary face PAR with $\pm 45^{\circ}$ scan angles is considered. The information about the surveillance and storm tracking tasks are visualized by the user in two displays. Parameters such as distance, area, volume, and time thresholds needed by the processes to initialize the framework are flexible and can be adjusted by the user. Because the weather environment evolves with time, it would be convenient for the user to change the inputs and/or outputs of the processes. Such freedom, however, is not considered in this work. The reflectivity obtained after the execution of the surveillance task (using either adaptive or conventional sensing) is sent to the storm cell identification and the overall process repeats again. A detailed description of each process is provided in Reinoso-Rondinel (2011).

3. Overview of quality measures for adaptive weather sensing

Two quality measures are proposed by Reinoso-Rondinel et al. (2010) to quantify the performance of adaptive weather sensing against conventional sensing and are briefly reviewed. For conventional sensing, the surveillance volume and the storm cells are being revisited at the same rate of U_C. In other words, the update time is the same for all storms. On the other hand, for adaptive weather sensing each storm cell and surveillance volume can be revisited at different rates and desirably faster rates. Thus, the revisit improvement factor for the j^{th} storm is defined by $I_j = U_C {U_j}^{-1}$, where U_j is the update time for the j^{th} storm. The revisit improvement factor represents the gain of revisits using adaptive over conventional sensing during the same period, while the data quality and spatial sampling are maintained. The "total" revisit improvement factor (I) for N storms is defined by the ratio of the total number of revisits using adaptive weather sensing over the one with conventional sensing during a given time period. The total revisit improvement factor is the average of the improvement factors for all storms being observed, and de-

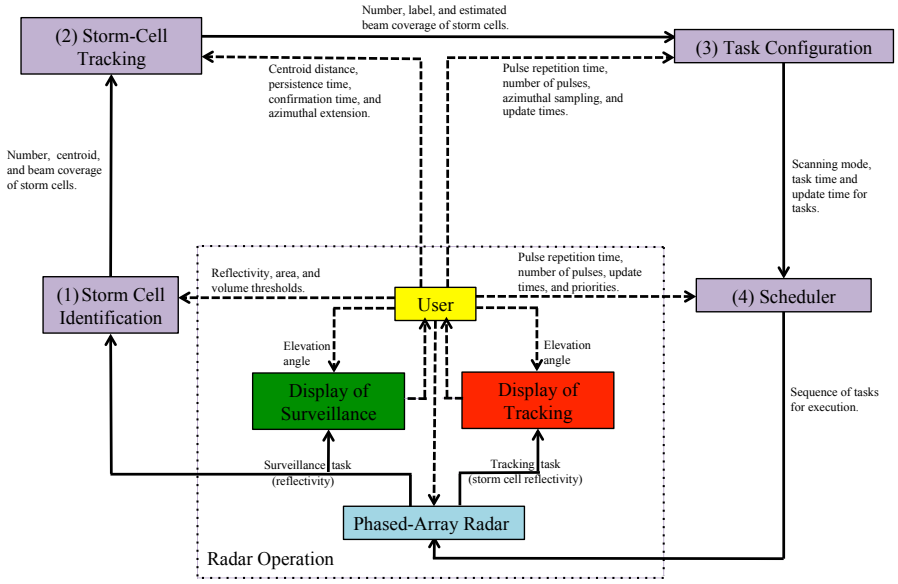

Figure 1: A block diagram of the closed-loop modular framework for adaptive weather sensing with four main processes: (1) storm cell identification, (2) storm-cell tracking, (3) task configuration, and (4) scheduler. The radar operation outlined by the dashed lines includes the PAR, the display of surveillance and tracking tasks, and the user inputs that are represented by the cyan, green, red, and yellow blocks, respectively.

pends on the number of cells and their update times. Improvement factors larger than 1 mean that adaptive sensing obtains more storm revisits than conventional sensing in an average sense.

If a radar dedicates too much time to one or a few of the tasks, other tasks may be significantly delayed. Thus, the acquisition time (A) is defined as the minimum time needed to execute each task at least once in the context of adaptive weather sensing. For example, if the radar is dedicated to tracking storms (i.e., the total tracking occupancy is high), the acquisition time will be determined by the completion of the surveillance task. In other words, within the acquisition time, tracking tasks may be executed multiple times. It is shown in Reinoso-Rondinel et al. (2010) that the acquisition time is determined by the largest update times among the surveillance and all the tracking tasks.

4. Optimal update times for tracking tasks

Requested update times are needed in the process of task configuration and subsequently the TB scheduler will schedule these tasks based on the requested update times for storm cells. If one or more storm cells are of interest, it is natural to assign fast update time to them to revisit them frequently. It is also important to design an automatic way to assign the update times of storm tracking tasks so that the total revisit improvement factor is maximized without exceeding a given acquisition time threshold. This can serve as a reference to the user about the optimal update times when no storm cells are of particular interest. As the size of storm cells increases or decreases, or some enter the radar's field of view and others exit it, the requested update times need to adapt so that the sum of storm tracking and surveillance occupancies reach 100%; i.e., the radar is fully loaded. The problem of assigning update times

for adaptive weather sensing is discussed next.

In this work, the optimization problem is formulated as follows. Given the task times of each storm tracking and surveillance task, what is the requested update time set $\mathcal{U}$ = $\{U_1, U_2, ...U_N, U_S\}$ for tracking and surveillance tasks such that the revisit improvement factor is maximized without exceeding an acquisition time threshold while maintaining a fully loaded radar?

$$\max_{\mathcal{U}} I \quad \text{subject to} \quad A \leq A_{th} \text{ and } O_T + O_S = 100\%, \tag{1}$$

where A_{th} is the acquisition time threshold, i.e., the maximum value allowed for any U_i. In this work, the maximum U_i was set equal to U_C=67 s and therefore, A_{th} = U_C. If U_C were much larger than 60 s, setting A_{th} = U_C would not longer be acceptable because the storm-cell tracking process assumed nominal update times of 60 s to predict the storm location and coverage for the next scan. In this case, either A_{th} should be set to a value less than U_C or the storm tracking parameters would need to be redetermined. Note that I, A, O_T, and O_S all depend on update times and therefore, (1) is a constrained, N + 1 dimensional, non-linear optimization problem. The optimal update times are obtained by solving (1) in the process of task configuration every time when the information of task times is updated. This method of assigning update times is termed optimal approach.

5. Demonstration and Verification

a. *Data Cases for Simulation of Adaptive Weather Observations*

Presently, the PAR at the National Weather Radar Testbed (NWRT) is not able to fully implement the proposed adaptive framework in real time. Thus, simulated observations from the archived WSR-88D data were used to test and verify the proposed framework for various weather scenarios. Although archived PAR cases with fast update times would be more suitable, the available types of storm environments were limited at the time we performed the analysis.

Table 1 illustrates the archived data cases from 4 WSR-88D radars that were used to test the adaptive weather sensing framework. These data cases were selected because they have been used in the literatures (e.g., Stumpf et al. 1998; Witt et al. 1998) to evaluate the performance of WSR-88D algorithms for hail, tornado, and mesocyclone detection. These selected data cases are not intended to comprehensively cover many events of weather phenomena. Nevertheless, it includes a variety of cases such as isolated supercells, minisupercells, tornadic, and squall line storms during the time periods described in Table 1. The WSR-88D reflectivity data at each elevation angle was linearly interpolated in time (gate-by-gate) to artificially obtain PAR observations with higher temporal resolution.

b. *Demonstration*

The data case observed by the KTLX radar on May 04 1999 during 0040 - 0320 UTC is used to demonstrate the adaptive weather sensing framework. First of all, the association of storm cells for a merging case is shown in Figure 2. At 0211 UTC, cells 1, 2, and 4 remained within the radar view, and their centroids are depicted on panel a) by the cyan, green, and light orange asterisks, respectively. In addition, a small cell was detected southwest of cell 2 and the process of confirmation begins. At 0212 UTC, cells 1 and 2 were connected at higher elevations and the storm identification process identified them as one cluster. Because the centroid of this cluster could not be associated with the centroid of neither cell 1 or cell 2, the process of confirmation for this new cluster began. Moreover, the process of persistence was initiated for cells 1 and 2 as shown on panel b). One minute later, at 0213 UTC, cells 1 and 2 were still being considered as two separated

Table 1: WSR-88D reflectivity data used to demonstrate the framework for adaptive weather sensing. Radar names are as follows: KTLX in Twin Lakes, OK; KMLB in Melbourne, FL; KOKX in New York City, NY; and KGLD in Goodland, KS. The WSR-88D radars used VCP 11.

Radar	Date	Period (UTC)	Storm Type
KTLX	1992 02 12	0410 - 0610	multicells
KTLX	1992 06 18	1840 - 2220	multicells with low-topped minisupercells
KTLX	1994 02 21	1950 - 2200	multicells
KTLX	1999 05 04	0002 - 0420	multicells with isolated supercells
KTLX	2003 04 19	2010 - 2250	multicells with isolated supercells
KTLX	2003 05 10	1700 - 2020	multicells and squall line
KTLX	2003 05 16	1720 - 1940	tornadoes along leading edge of squall line
KTLX	2003 05 19	2218 - 2345	multicells with isolated supercells
KMLB	1992 06 02	1810 - 2010	multicells with minisupercells
KMLB	1992 06 12	1920 - 2300	supercells (near range), isolated supercells
KOKX	1995 06 20	1910 - 2050	multicells with isolated supercells
KGLD	1995 05 12	0003 - 0145	multicells with high precipitation supercells

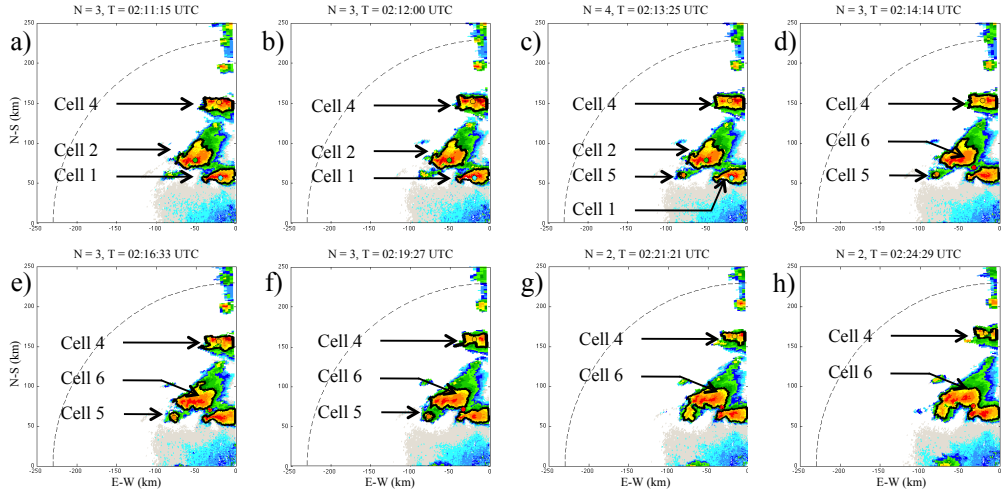

Figure 2: Association during the merging of storm cells. At 0211 UTC, three cells are defined and labeled as cells 1, 2, and 4 as shown on panel a). Storm cells at 0212 UTC are associated with these at 0211 UTC and are shown on panel b). At 0213 UTC a new cell is confirmed and is labeled as cell 5 (panel c). One minute later, cells 1 and 2 merged and created a new cell, cell 6 as shown on panel d). Cells 4, 5, and 6 continued to develop as shown on panels e) and f). At 0221 UTC, cell 5 merged with cell 6 (panel g). Finally, the storm cells at 0224 UTC are associated with cells at 0221 UTC (panel h).

clusters, while the small cell detected at 0211 UTC was now confirmed as a new cell, cell 5 (panel c). Cell 4 continued developing. At 0214 UTC, the cluster obtained by the merging of cells 1 and 2 was confirmed, producing a new cell (cell 6), while the persistence of cells 1 and 2 was terminated (panel d). From 0214 to 0216 UTC, a smooth transition of storm cells can be observed in panel e). At 0219 UTC, cell 5 could not be associated with cells 4 or 6 because it is now part of cell 6. As a result, the process of persistence for cell 5 began, as shown on panel f). Two minutes later, at 0221 UTC, the persistence process for cell 5 was terminated, so cell 5 became a part of cell 6, as shown on panel g). This merging process is different from the one that happened at 0214 UTC in which cells 1 and 2 could not be associated with the new cluster involving them. Thus, they merged and created the storm cell 6. On the other hand, when cells 5 and 6 were defined as one cluster, cell 6 was associated to that cluster. As a result, the merging of cells 5 and 6 did not create a new cluster. At 0224 UTC, the reflectivity components of cell 6 look more connected while cell 4 starts to decay as shown on panel h).

The established track of storm centroids from 0040 UTC to 0320 UTC is shown in Figure 3. A total of thirteen storm cells were identified and associated during the simulation period. For this data case, the long tracks generally occurred for the cells having an area and volume considerable larger than the thresholds. Also, storm cells with large reflectivity values contribute to develop long displacements because they keep converging and evolving. On the other hand, storm cells with short tracks can be due to one or more of the following reasons. First, the displacement of cells could be short because the time from the moment cells were defined until they merged is short. Second, the location of defined cells could be close to the boundaries of the radar scene. Finally, short displacements could occur simply because storm cells decay rapidly (not including the case of merging).

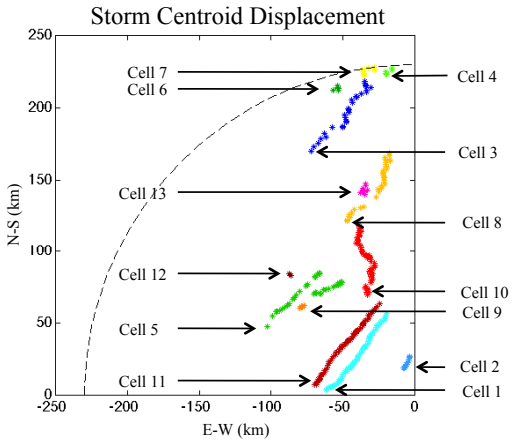

Figure 3: Storm centroid displacement during the period of 0040 - 0320 UTC. Thirteen cells were defined within the radar scene. The centroid displacement of each cell is represented by an asterisk mark using thirteen colors. The centroid of each cell is labeled as cells 1 through 13. It is apparent that the storm cells were moving northeasterly.

The theoretical acquisition time and total revisit improvement factor for this case are shown in the panels a) and b) of Figure 4, respectively. The quality measures from the opti-

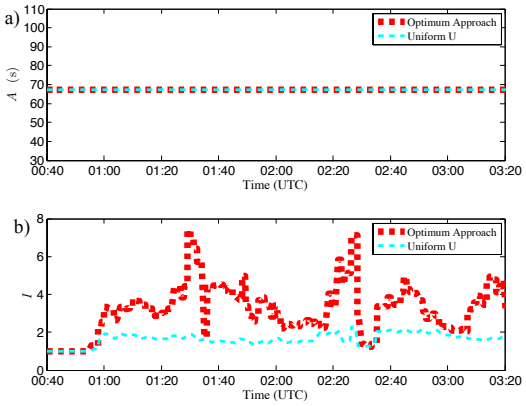

Figure 4: The theoretical acquisition time and the revisit improvement factor are shown on panel a) and b), respectively. Quality measures from the optimum approach and uniform update time criterion are denoted by the red and cyan dashed lines, respectively.

mum approach for assigning update times are

denoted by red dashed lines. In addition, a simple method of assigning updates times was also employed, where the update times for all tracking tasks are equal and the radar is fully loaded. This is termed uniform update time criterion and the resulted improvement factor and acquisition time are denoted by cyan dashed lines. As can be seen on panel a), the acquisition times for the optimum approach and uniform update time criterion are the same as the surveillance update time U_S = 67 s. Since the acquisition time was defined as the maximum update time among storm tracking and surveillance tasks, the maximum update time is determined by the surveillance task.

It is clear from Figure 4 that the adaptive weather sensing framework can provide revisits of storms at a higher rate comparing to conventional sensing for most of times. The impact of update times is evident that optimum approach often produces the total revisit improvement factor between two and four comparing to the improvement factor of approximately two from the uniform update time criterion. For example, at 0130 UTC, the optimum approach achieves the highest revisit improvement factor, when the three storm cells were identified with task times of T_1 = 20 s, T_5 = 13 s, and T_6 = 1.5 s, respectively. Update times of the three cells assigned by the optimum approach were U_1 = 67 s, U_5 = 67 s, and U_6 = 3.3 s, respectively. Note that the smallest update time is assigned to storm cell 6, which has the smallest task time. In other words, the revisit improvement factor for storm cell 6 with smallest size is as high as approximately 20. As a result, the total revisit improvement factor is 7.4. For the uniform update time criterion, the update time assigned to each storm cell is 39 s, which results the total revisit improvement factor of only two.

It is interesting to point that the optimum approach has the tendency to assign small update times for smaller cells. This can be demonstrated by examining the case of two storm cells. The total revisit improvement factor can be derived in the following form base on the constrains of 100% total occupancy.

$$I = I_1 \frac{T_2 - T_1}{2T_2} + \frac{O_T U_C}{2T_2} \tag{2}$$

where T_1 and T_2 are the given task times for cells 1 and 2, and I_1 is the revisit improvement factor for cell 1. Let's assume that cell 1 is the larger storm (i.e., $T_2 - T_1 < 0$). Note that we currently require the maximum update time for each task not to be larger than the update time for conventional sensing (U_C), which results in the minimum improvement factor of I_1 to be one. It can be observed from (2) that I is a linear function of I_1 and has a maximum value of $\frac{T_2-T_1}{2T_2} + \frac{O_T U_C}{2T_2}$ at $I_1 = 1$. It is the reason why the optimum approach produces the improvement factor of one for the larger storm, while maximizing the improvement factor for the other smaller storm. In other words, the large storm will be revisited at a rate of conventional sensing, while the smaller storm will be revisited as frequently as the constrains are not violated. This might be mitigated if a different quality measure from the total revisit improvement factor is used. Furthermore, it can be observed from (2) that if the task times for both cells are equal ($T_1 = T_2 = T$), the total improvement factor is determined by $I = \frac{O_T U_C}{2T}$ and is only a function of task time. Consequently, the optimum approach often selects $U_1 = U_2$ in this case.

We have examined the cases of two storm cells during the time intervals of 0230-0245 and 0250-0308 UTC from the optimum approach. A scattering plot of the total revisit improvement factor (I) multiplied by the task time for smaller cell (T_2) and the task time difference ($T_1 - T_2$) is shown in Figure 5. Note that during both intervals only two storm cell are identified. The linear relationship between IT_2 and $T_1 - T_2$, as indicates in (2), is clearly shown. In other words, the larger storm maintains improvement factor of one while for the other cell, the smaller the cell the larger the improvement factor is obtained.

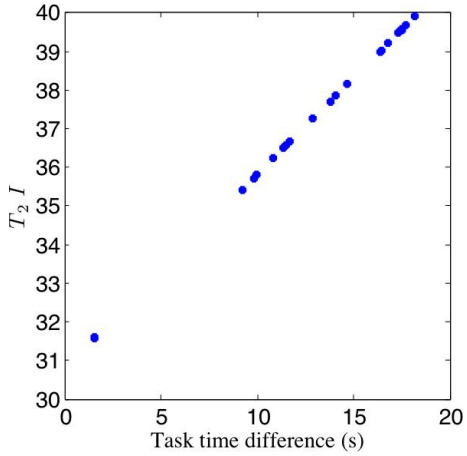

Figure 5: Total revisit improvement factors from the optimum approach as a function of the task time difference. The x axis represents the task time difference between storm cells 10 and 11 over the time intervals of 0230-0245 and 0250-0308 UTC, approximately. The y axis represents the total revisit improvement factors from the optimum approach multiplied by T_2 during both time intervals.

c. *Statistical Analysis*

It is of interest to investigate how the adaptive weather sensing performs during different storm environments. First, we classified the storm environments based on the number of storm cells and their total coverage. The storm coverage is divided into nine intervals as shown in Table 2, where the coverage indexes and

Table 2: Storm coverage intervals.

Coverage Index	Coverage Interval (%)
C_1	(0, 17)
C_2	[17, 28)
C_3	[28, 39)
C_4	[39, 50)
C_5	[50, 61)
C_6	[61, 72)
C_7	[72, 83)
C_8	[83, 92]
C_9	$>$ 92

coverage intervals of storm cells are given on the left and right columns, respectively. Because the conventional sensing mode is triggered if the sum of the tracking and surveillance task times is larger than U_C, the maximum sum of task times for tracking tasks is given by U_C - T_S. Consequently, the maximum storm coverage for the adaptive sensing mode is 92% so it is the upper limit of the coverage index C_8. Storm environments with coverage larger than 92% are indicated by the coverage index C_9. The 12 archived data cases described in Table 1 were used to simulate the adaptive weather sensing framework with the optimal approach for assigning update times. A total of 1352 storm environment cases over the 12 data cases were analyzed. The estimated acquisition time was calculated by counting the minimum time in which all the tasks were executed at least once. The estimated revisit improvement factor was calculated by summing the number of tracking executions over the estimated acquisition time. It is important to mention that both quality measures were obtained at every acquisition time window. The resulted quality measures of estimated total revisit improvement factor and acquisition time were grouped by the number of storm cells and the coverage index. The number of storm environments in each group is presented in Figure 6a. The mean of total revisit improvement factor and acquisition time are shown in Figure 6b and c, respectively. It can be observed that storm environments with more than 5 storm cells or with coverage indexes larger than C_7 are not observed within the 12 data cases. It is evident that the mean revisit improvement factor of higher than 10 can be observed for smaller coverage (C_1). The improvement of revisits decreases as the coverage increases. The dependence of storm numbers for the revisit improvement factor is not apparent. The mean of revisit improvement factor over 1352 storm environments is approximately 4.3. Moreover, the mean of acquisition time over all storm environment classes is approximately 70 s, which approximately agrees the value of U_C = 67 s. The standard deviation of acquisition time is 7.7 s. Acquisition times larger or smaller than 70 s could happen dur-

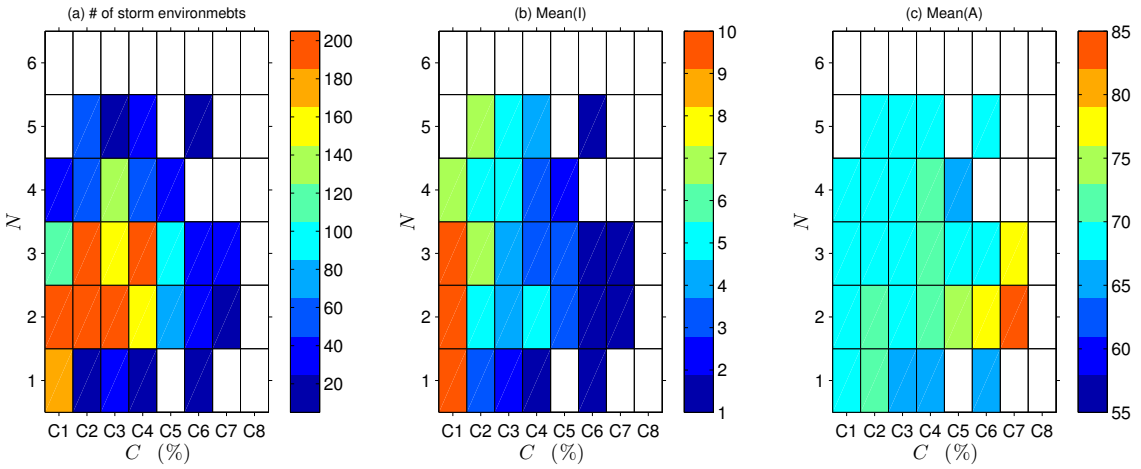

Figure 6: Panel a), number of cases for each storm environment class classified by the coverage index and number of storm cells. Panel b), average revisit improvement factors over each storm environment class. Panel c), average acquisition times over each storm environment class.

ing periods when storm cells entered to or exit the radar view, which caused TB scheduler to lose balance.

6. Summary and conclusions

In summary, an adaptive weather sensing framework was developed and demonstrated. An approach was designed to automatically assign update times to maximize the benefits of adaptive weather sensing. Moreover, the performance of such approach was analyzed using simulation of 12 data cases, which covers a range of different weather events. Statistical results have shown that the adaptive sensing with optimum approach can revisit storm cells 4.3 times more often than using conventional sensing while keeping the acquisition time near 70 s. It is important to highlight that during the simulations of the adaptive weather sensing framework, the quality of the data over storm regions were the same as with conventional sensing.

Acknowledgement This work was primarily supported by NOAA/NSSL under Cooperative Agreement NA17RJ1227.

References

Crum, T. D. and R. L. Alberty, 1993: The WSR-88D and the WSR-88D operational support facility. *Bull. Amer. Meteor. Soc.*, **74**, 1669–1687.

Reinoso-Rondinel, R., 2011: *A framework for Adaptive Weather Sensing Using Phased-Array Radar*. Master's thesis, University of Oklahoma.

Reinoso-Rondinel, R., T.-Y. Yu, and S. Torres, 2010: Multifunction phased-array radar: Time balance scheduler for adaptive weather sensing. *J. Atmos. Oceanic Technol.*, **27**, 1854–1867.

Stumpf, G. J., A. Witt, E. D. Mitchell, P. L. Spencer, J. T. Johnson, M. D. Eilts, K. W. Thomas, and D. W. Burgess, 1998: The national severe storms laboratory mesocyclone detection algorithms for the WSR-88D. *Wea. Forecasting*, **13**, 304–326.

Witt, A., M. D. Eilts, G. J. Stumpf, J. T. Johnson, E. D. Mitchell, and K. W. Thomas, 1998: An enhanced hail detection algorithm for the WSR-88D. *Wea. Forecasting*, **13**, 286–303.